

Journal of Biomedical Optics

BiomedicalOptics.SPIEDigitalLibrary.org

Retrieving the axial position of fluorescent light emitting spots by shearing interferometry

Johannes Schindler
Philipp Schau
Nicole Brodhag
Karsten Frenner
Wolfgang Osten

SPIE.

Johannes Schindler, Philipp Schau, Nicole Brodhag, Karsten Frenner, Wolfgang Osten, "Retrieving the axial position of fluorescent light emitting spots by shearing interferometry," *J. Biomed. Opt.* **21**(12), 125009 (2016), doi: 10.1117/1.JBO.21.12.125009.

Retrieving the axial position of fluorescent light emitting spots by shearing interferometry

Johannes Schindler,* Philipp Schau, Nicole Brodhag, Karsten Frenner and Wolfgang Osten

University of Stuttgart, Institut für Technische Optik, Pfaffenwaldring 9, 70569 Stuttgart, Germany

Abstract. A method for the depth-resolved detection of fluorescent radiation based on imaging of an interference pattern of two intersecting beams and shearing interferometry is presented. The illumination setup provides the local addressing of the excitation of fluorescence and a coarse confinement of the excitation volume in axial and lateral directions. The reconstruction of the depth relies on the measurement of the phase of the fluorescent wave fronts. Their curvature is directly related to the distance of a source to the focus of the imaging system. Access to the phase information is enabled by a lateral shearing interferometer based on a Michelson setup. This allows the evaluation of interference signals even for spatially and temporally incoherent light such as emitted by fluorophors. An analytical signal model is presented and the relations for obtaining the depth information are derived. Measurements of reference samples with different concentrations and spatial distributions of fluorophors and scatterers prove the experimental feasibility of the method. In a setup optimized for flexibility and operating in the visible range, sufficiently large interference signals are recorded for scatterers placed in depths in the range of hundred micrometers below the surface in a material with scattering properties comparable to dental enamel. © The Authors. Published by SPIE under a Creative Commons Attribution 3.0 Unported License. Distribution or reproduction of this work in whole or in part requires full attribution of the original publication, including its DOI. [DOI: [10.1117/1.JBO.21.12.125009](https://doi.org/10.1117/1.JBO.21.12.125009)]

Keywords: fluorescence; microscopy; shearing; interferometry; scattering.

Paper 160736PR received Oct. 25, 2016; accepted for publication Dec. 7, 2016; published online Dec. 28, 2016.

1 Introduction

Microscopy methods for noninvasive diagnostics are limited by the strong scattering encountered in biological materials. This leads to disturbing background signals, weak signal-to-noise ratio, and image degradation. The situation is even worse when one needs to detect information about the position of a signal source in all three spatial dimensions. Light from in-focus as well as from regions far out-of-focus contributes to the recorded signal. Hence, some sort of discrimination between the desired signal and contributions arising from scattering in the rest of the sample is needed. Many diagnostic applications require such dimensional measurements: in the classification of skin cancer, the extent of a tumor in the vertical direction is directly linked to its development over time.¹ Hence, three-dimensional (3-D) data about the location of certain structures, in particular along the z -axis, could contribute to a better classification of images, the recognition of features, and the automated segmentation of malign and benign areas. In applications where optical methods aid in the determination of tumor margins or even serve as feedback during surgery,² dimensional information is obviously of crucial importance.

Two widely used approaches exist. In optical coherence tomography (OCT), the depth information is obtained by the interference signal of the reflected light with a reference beam. The small coherence length of the light source limits the region along the optical axis in which an interference signal is detected. This interferometric depth detection gives the advantage of decoupling axial and lateral resolution. It is the method of choice for the imaging of 3-D structures up to a depth of 1 mm.³ Yet, a main limitation remains: the method cannot be

applied to fluorescent light as there is no correlation and hence no coherence between excitation and emitted light. In the context of tumor diagnostics, another limitation arises: the method is more sensitive to variations in refractive index than to concentrations of marker materials; hence, this approach of increasing contrast between different types of tissue cannot be fully exploited.

A second class of approaches physically implements a depth discrimination and uses fluorescent light. In fluorescence microscopy, the usage of suitable bandpass filters provides a good selectivity between reflected and scattered excitation light and the fluorescence signal. Typical implementations are multi-photon fluorescence microscopy,⁴ light-sheet microscopy,⁵ fluorescence lifetime imaging,⁶ or confocal microscopy.⁷ These methods are designed for the use of fluorescent marker materials. The depth information is obtained by restricting both excitation and detection to a small volume in the vicinity of the focus. The depth resolution is directly related to the properties of the illumination and imaging optics instead of the evaluation of an interference signal. As only light close to the focus contributes to the signal at the detector, a scanning in all three dimensions is necessary; during the scanning, in each step only a part of the fluorescent light is recorded. Light sheet microscopy can be extended by fusion of images with structured and uniform illumination for the suppression of the background signal.⁸

The structured illumination microscopy realizes a depth discrimination by imaging a pattern to the focal plane and exploits the fact that only in the vicinity of the focus is this pattern imaged sharply. In combination with the computational evaluation of images recorded for different lateral positions of the pattern, this provides a precise vertical localization.⁹

The short coherence length of fluorescent light prohibits an interferometric evaluation with a reference wave such as in OCT, yet access to the phase of a fluorescent signal can be gained by

*Address all correspondence to: Johannes Schindler, E-mail: schindler@ito.uni-stuttgart.de

shearing interferometry. A beam-split copy of the object wave serves as the reference. Hence, the optical paths are balanced and interference is observed in spite of the short coherence length of fluorescent light. As interference takes place between waves emerging from the same point, no spatial coherence is required. Different setups and applications are built on this principle. The so-called Fresnel incoherent correlation holography uses a spatial light modulator for realizing both the shear and phase shifting procedures.^{10,11} This enables the reconstruction of the microscopic image in different z -planes and yields information about the 3-D position of different structures within a full-field image. A setup for off-axis holography based on a Sagnac interferometer has been reported by Wan et al.¹² In a holographic camera proposed by Kim,¹³ a Michelson interferometer with one curved mirror realizes the interference between the two sheared wave fronts. In the so-called quadriwave lateral shearing interferometry,^{14,15} shears in two orthogonal directions are realized simultaneously by using a modified Hartmann mask for wave front sensing. The combination of the method for the recording of the phase with the direct stochastic optical reconstruction microscopy imaging technique enabled a very precise localization of gold nanoparticles in the nanometer range.¹⁶ Lateral shearing setups based on point diffracted spherical waves¹⁷ and a wedged glass plate¹⁸ have been reported for the measurement of 3-D distances in the range of several millimeters¹⁸ up to several hundred millimeters.¹⁷

In this work, a phase-sensitive method for the depth-resolved detection of fluorescent light based on the combination of illumination with an interference pattern arising from two intersecting beams with shearing interferometry is proposed. This aims at combining the advantages of fluorescence detection and using highly sensitive interferometric signals for the depth evaluation. In addition to using fluorescence band-pass filters, the contribution of scattered light is suppressed by locally addressing the excitation of fluorescent light and limiting the excitation volume by the geometry of the illumination setup. The implementation of a phase shifting procedure allows efficient separation of the interferometric signal from the incoherent background, which is of particular importance for recording signals from a scattering environment. However, this comes at the expense

of an increased time for image acquisition as at least three phase-shifted images have to be recorded.

While the setup has a similar structure as some holographic methods, the focus of this work is the measurement of the axial position of a fluorescent light source in a scattering environment rather than imaging. In contrast to scanning methods such as confocal or multiphoton fluorescence microscopy, signals arising from regions far out-of-focus can be used, so scanning along the vertical direction is avoided. The lateral shearing is implemented in a Michelson interferometer with a tilted mirror that is integrated into a conventional microscope. Compared to the shearing based on specialized components such as the modified Hartmann mask^{14,15} or a spatial light modulator,¹³ the optics in the detection consists of standard catalog components.

As opposed to the imaging approaches of scanning fluorescence microscopy, the determination of the 3-D location of a fluorescent source requires a signal model for the interference signal. An analytical model for the measurement of the fluorophor positions is derived and validated. For the purpose of proving the feasibility of the proposed method, specifically designed reference samples with well-characterized optical properties are examined. Different experimental configurations allow investigation of the performance of the method. Key requirements are the feasibility of obtaining phase information of incoherent light, the separation of the signal from scattering background, and the quantitative assessment of the depth reconstruction.

2 Experimental Setup

The experimental approach relies on combining a dedicated illumination setup with a shearing interferometer for the phase reconstruction. The basis for the setup is a usual fluorescence microscope in epi-illumination configuration, see Fig. 1. The bandpass filters F1, F2 are adapted to the fluorophor rhodamine 6G with absorption and emission peaks at 532 and 552 nm, respectively.¹⁹ To preserve the flexibility with respect to a working distance covering several hundred micrometers, a microscope objective with moderate numerical aperture of 0.4 and 20 \times magnification is used.

The creation of an interference pattern in the focal plane can be achieved by illuminating with two beams separated in the

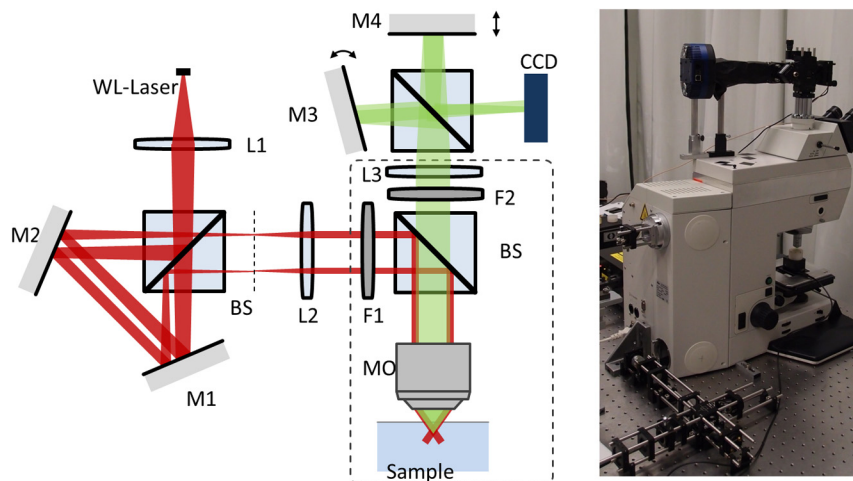


Fig. 1 Schematic layout and photograph of the experimental setup. Ls, Lenses; Ms, mirrors; BS, beam splitters; Fs, bandpass filters; MO, microscope objective. The dashed line corresponds to the housing of the microscope.

pupil plane of the microscope. This leads to two light cones intersecting each other under an angle in the focal plane after passing the microscope objective. Translating one of the mirrors M1, M2 in axial direction allows the adjustment of the intersection angle. For the current setup, intersection angles in the order of 5 to 20 are realized. Due to the intersecting beams, the volume in which fluorescence is excited is significantly decreased, yielding a coarse depth restriction in the axial direction in the range of a hundred microns. The special case of overlapping beams corresponds to the illumination of a confocal microscope. As an additional benefit, due to interference between the overlapping beams, the intensity in the focal plane can be increased by a factor of two. The Sagnac setup is common-path, hence facilitating alignment and increasing robustness.

The interferometric phase detection is realized by integrating a Michelson interferometer into the imaging path of the microscope. Tilting the mirror M3 allows implementation of a lateral shear. Again, the common path nature of the setup ensures robustness against alignment errors and vibrations. Up to the small tilt of the mirror M3, it is possible to balance the path lengths in the interferometer so that interference patterns are obtained even for light sources with short temporal coherence such as fluorophors. In the case of rhodamine 6G, the coherence length is in the range of $10 \mu\text{m}$ ¹⁹ or even longer after passing the filter F2. The tilt of the mirror M3 leads to the superposition of the incoming master wave front with a laterally shifted copy of itself with typical shear distances in the range of a few microns. Thus, it is possible to match the optical path lengths of the interfering beams up to a distance smaller than their coherence length.

For the detection, a CCD cooled camera is employed for low-noise images even at long integration times. The mirror M4 is mounted on a piezodriven translation stage, which allows application of a temporal phase shifting procedure.

3 Phase Reconstruction and Depth Resolution

3.1 Signal Model and Phase Reconstruction

The signal at the detector arising from interference of the two sheared wave fronts is modeled by the usual equation for two-beam interference

$$I(x, y; \delta z) = 0.5I_0(x, y; \delta z) \times \left\{ 1 + \gamma(x, y) \cos \left[\frac{2\pi}{\lambda} V(x, y; \delta z) + \phi_0 \right] \right\}, \quad (1)$$

where x, y denote the position of a pixel at the detector, I_0 is the intensity at the entrance of the Michelson interferometer, V is the optical path length difference between the master and the sheared wave front, γ is the pixel-wise modulation or fringe contrast, and ϕ_0 is an undetermined phase offset. The widely used Schwider–Hariharan algorithm^{20,21} enables obtaining the phase difference V and the contrast γ from multiple images recorded at different phase shifts introduced by axially shifting the mirror M3. A standard unwrapping procedure²² allows obtaining the continuous phase V . The fringe contrast γ can be considered as a measure for the quality of the interference signal and the validity of the employed model. Factors leading to a decrease of the contrast are the finite extent of the

fluorophor distribution, the finite bandwidth of the fluorescent radiation, a remaining optical path difference between the two arms of the Michelson interferometer as well as the background of scattered light. The parameter δz denotes the axial distance between the focus of the sheared wave fronts and the detector. This is directly related to the distance of the fluorophor to the focus of the microscope objective by the magnification of the imaging system, consisting of microscope objective, tube lens, and imaging optics.

In the following examination of the difference of the optical path lengths V between master and sheared wave front, the coordinate system is oriented such that the direction of the shear is along the x -axis. V can be expressed as

$$V = W(x, y) - W(x - s_x, y) + k \cdot s_x \cdot x. \quad (2)$$

k is a constant depending on the exact geometry of the setup (positions and dimensions of beam splitter and imaging optics), which is calibrated along with the shear distance. The wave fronts W are modeled as spherical wave fronts that can be expanded into Zernike polynomials

$$W = \sum_n c_n Z_n(x, y). \quad (3)$$

Such an expansion of the spherical wave front into Zernike polynomials has been worked out by Chu and Kim¹⁷, and the following relation between the amount of defocussing δz and the coefficients of astigmatism and power arises if the expansion is truncated after the first six Zernike polynomials

$$\delta z = \frac{1}{4 \cdot c_5 + 2\sqrt{c_4^2 + c_6^2}}. \quad (4)$$

In principle, one could obtain the wave front W according to the method of Rimmer and Wyant²³ by numerically integrating the difference V for two shears in orthogonal directions. This would also allow using the expansion in Ref. 17 for a reconstruction of the x - and y -positions. In the case of the method presented here, two simplifications can be applied. First, due to the nature of the illumination, the excitation takes place only in a small vicinity of the focus, i.e., on the optical axis such that the field-dependent aberration of astigmatism can be neglected. Hence, a shear in only one direction is sufficient. Second, only small shears in the range of a few micrometers are applied. Hence, terms of quadratic or higher order in the shear s_x can be neglected. This enables the direct relation of the Zernike coefficients of the difference phase V to those of the master wave front W by comparing coefficients in the following equation:

$$V(x, y) = c_1 \cdot s_x + c_2 \cdot s_y + 2c_5 \cdot s_x x + 2c_5 \cdot s_y y - c_5(s_x^2 + s_y^2). \quad (5)$$

V can also be expanded into Zernike polynomials: $V = \sum_n d_n Z_n(x, y)$. Comparing the coefficients d_n of V with Eq. (5) yields that the distance δz can be directly related to the tilt coefficient d_2 of the wave front V

$$\delta z = \frac{s_x}{2 \cdot d_2 - k}. \quad (6)$$

4 Experimental Results

The feasibility of the method is demonstrated by measurements in different configurations of increasing complexity. First, the validity of the model is tested at point-like fluorescent light sources. Second, spatially extended fluorescent light sources and a measurement range of several hundred microns in a weakly scattering material are considered. In the last configuration, a scattering phantom with isolated inclusions of fluorophores is examined.

4.1 Isolated Fluorophores

In the first step, the capability of the method for the depth-resolved detection of fluorescent light is demonstrated. Single crystals of rhodamine 6G with sizes in the range of a few microns are placed on a sample holder. This sample offers the advantage that fluorescent wave fronts arising from well-defined lateral and axial positions are obtained, where the axial position can be precisely set by means of the stage of the microscope.

In Fig. 2, the raw phase data obtained by the phase shifting procedure are plotted for different distances of a fluorescent particle to the focus. The data illustrate the measurement principle with the tendency of increasing fringe distance with increasing depth. In spite of the short temporal coherence of the fluorescent radiation, clear and quantitatively evaluable interference signals can be obtained. The signal quality tends to improve for larger distances. This can be ascribed to two effects: the influence of parasitic signal components, e.g., reflections of the isotropically emitted fluorescent light at the back side of the sample holder, or residual excitation light is much more pronounced in the vicinity of the focus. Additionally, due to the larger fringe spacing at larger distances, the noisy components tend to average out better. The inset of Fig. 3 shows the achievable axial resolution for point-like fluorescent light sources. Due to the evaluation of the phase, displacements of single micrometers could clearly be resolved.

The quantitative results for the reconstruction of the axial position are shown in Fig. 3. An agreement with the nominal values of the microscope stage within the range of $10 \mu\text{m}$, corresponding to relative deviations of a few percent, can be found. The remaining deviations can be ascribed to perturbances in

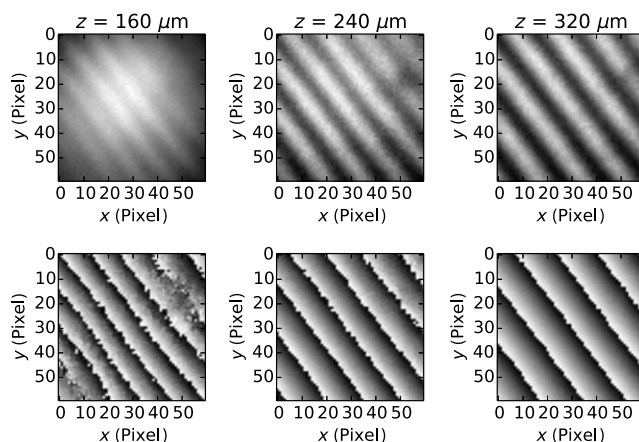


Fig 2 Fluorescent intensity images with interference patterns (top row) and results of phase shifting (bottom row) for fluorescent particles at different distances to focus.

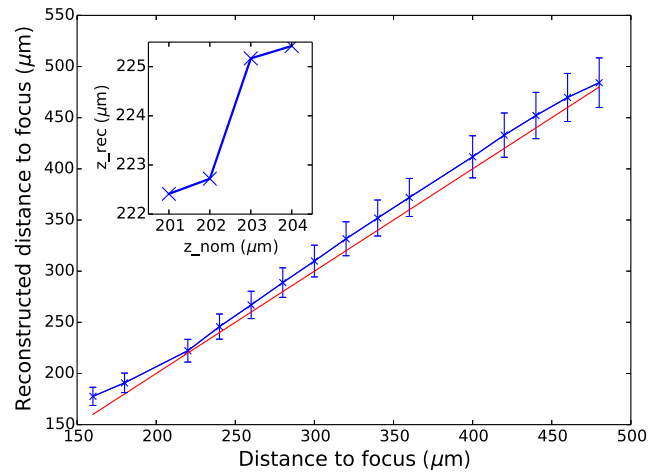


Fig. 3 Validation of depth reconstruction at fluorescent sample and test of axial resolution (inset).

the raw signal, such as reflections at the back side of the sample holder, residual parts of excitation light entering the detection part, uncertainties in determination of the shear distance, the finite bandwidth of the fluorescent radiation, and aberrations in the imaging system. The error bars are computed by taking into account the dominant error sources appearing in Eq. (6). The shearing distance is calibrated by recording interferograms of a point-like source in several known depths and can be determined with a relative accuracy of 5%, which leads to an error contribution proportional to the reconstructed depth. The error in tilt coefficient of the sheared wave front can be estimated by the phase noise in the raw data and the conditioning of the fit.

4.2 Extended Distributions of Fluorophores

The applicability of the method to samples with extended regions of fluorophores is investigated in a sample containing a layer of fluorescent material with a thickness of 10 to $15 \mu\text{m}$, which is tilted by 3° with respect to the surface. Hence, different lateral positions of the sample correspond to different depths of the fluorophores. Figure 4 shows the raw signal of a depth of $550 \mu\text{m}$ and the corresponding fringe contrast. In spite of the large extent of the fluorescing volume and the lack of spatial incoherence, an interference pattern with a fringe contrast in the range of 30% is recorded. It is assumed that this is due to the illumination, which confines the excitation of

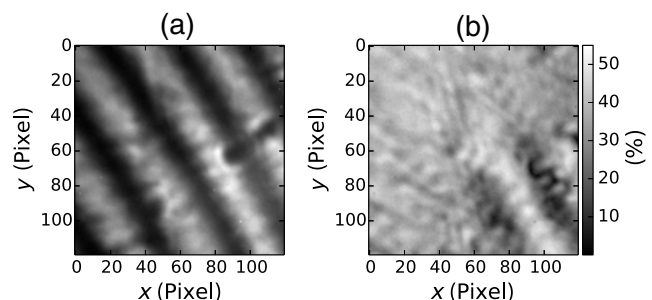


Fig. 4 Raw fluorescent intensity image with (a) interference pattern and (b) fringe contrast for fluorescent layer at a depth of $550 \mu\text{m}$.

fluorescent radiation both laterally and axially. This is also in agreement with previous simulation results,²⁴ where the propagation of the excitation and the fluorescent light has been modeled based on numerical solutions of the Maxwell equations and similar values for the resulting fringe contrast have been obtained.

Figure 5 shows the comparison between the nominal values and the result for the reconstructed depths for different positions along the profile. The reconstructed values agree with the nominal ones within the range of the uncertainty for the actual layer, corresponding to a relative error of around 10%. It is to be noted that no spatial coherence is required in the formation of the shearing interference signal, as interference takes place between parts of the wave front emerging from the same point in space. The sole effect of an extended source distribution is a decrease in contrast.

4.3 Fluorescent Inclusions in a Scattering Material

The depth reconstruction in a setup closer to possible applications is demonstrated with measurements at a scattering phantom. The principles of the production and characterization of the optical properties of similar phantoms are described by Krauter et al.²⁵ The phantom consists of a scattering matrix material with a scattering coefficient of $\mu_s = 2/\text{mm}$ and a refractive index of $n = 1.56$ with inclusions of rhodamine 6G with sizes in the range of 10 to 100 μm . The fluorescent inclusions are located in randomly distributed positions within the sample. The mean distance between the inclusions is adjusted, so only one fluorescent inclusion is placed in the field of view. To systematically investigate the depth reconstruction over a large measurement range, a single fluorescent inclusion in the phantom has been selected and has been positioned in different vertical positions. Hence, the distance to the focus of the microscope objective could be precisely controlled. Figure 6 shows the results of the phase shifting procedure for a set of different distances to the focus. In spite of the scattering, clear and well-evaluatable interference patterns can be observed, and the data visualize the relation between defocusing and decreasing fringe density. The results show a similar signal quality as in Fig. 2, which underlines the efficiency of the phase shifting procedure in separating the interference signal from the scattering background. To quantify the signal quality, Fig. 7 shows one of the recorded frames and the fringe contrast obtained during the phase shifting

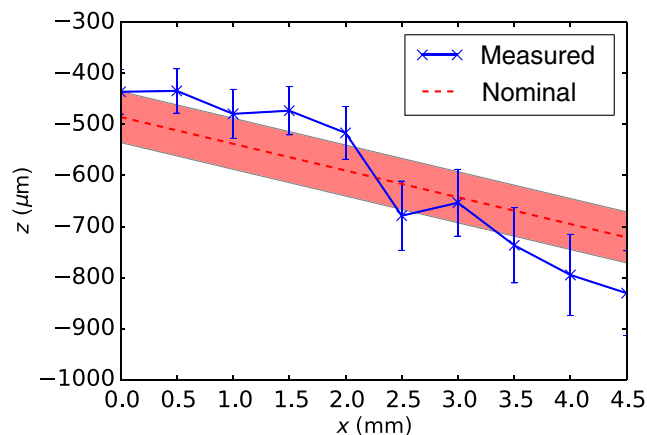


Fig. 5 Validation of depth reconstruction at fluorescent layer.

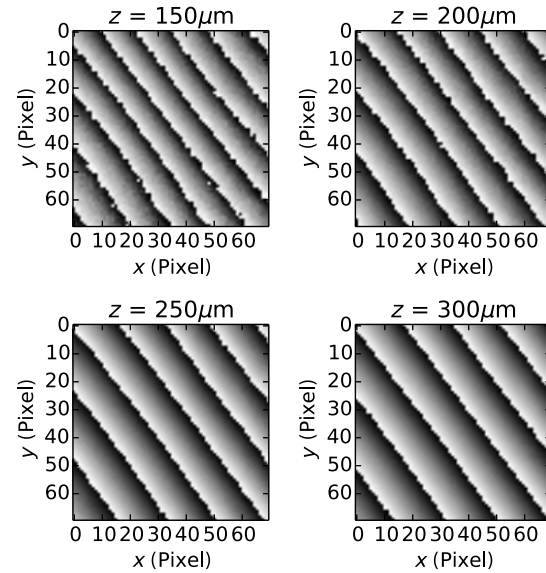


Fig. 6 Results of phase shifting for different vertical positions of fluorescent inclusion. This illustrates the relation described by Eq. (6). The spacing of the fringes increases with increasing distance of the fluorescent light source to the focus. The interference patterns correspond to tilted wave fronts. This is in agreement with the approximation applied to Eq. (5), i.e., that the difference of parabolic wave fronts can be approximated as a tilted wave front for a small shear distance.

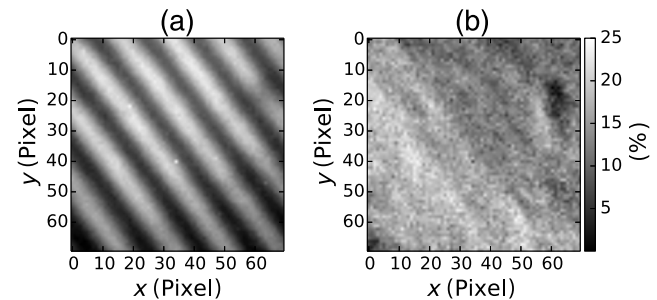


Fig. 7 Interference pattern (a) and modulation contrast γ (b) for a depth for 250 μm . A fringe contrast in the range of 20% is observed over the full field of view, which is sufficient for a quantitative evaluation of the phase.

procedure and characterizes the quality of the interferometric signal. In spite of the clearly visible noisy scattering background, a contrast in the range of 15% to 20% can be obtained over the full field of view with local perturbations due to impurities in the setup and inhomogeneities in the sample. The knowledge of the fringe contrast can be exploited to locally mask out regions of the image with poor signal quality. Again, the results are in good qualitative agreement with previous simulations,²⁴ which have also shown that a sufficient contrast survives even for penetration depths of 500 μm . Due to the increased fringe spacing for larger depths, an effect of averaging out of scattering components has been found, which leads to even decreased noise levels.

Figure 8 shows the reconstructed sample with the nominal axial positions of the fluorescent inclusion. Compared to the case of the single particle on the sample holder, the difference to the nominal values is increased but still in a range of relative

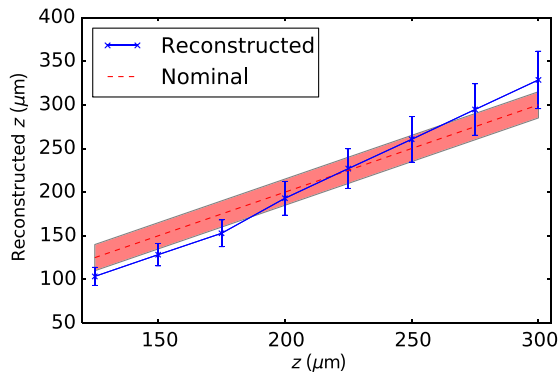


Fig. 8 Validation of depth reconstruction at sample with fluorescent inclusions.

deviations of 10% to 20%. Several factors contribute to these larger deviations. The uncertainty of the nominal values is increased due to the scattering and the spatial extent of the fluorescent inclusions. Compared to the case of the isolated fluorophores, the integration times are two orders of magnitude longer. Intensity fluctuations in the light source are more pronounced and lead to errors in the phase shifting procedure. For smaller values of z , the reconstructed values turn out to be too small and for larger values, too large. This could be due to a remaining inaccuracy in the determination of the shear distance s_x in Eq. (6), which would lead to an error in the slope of the reconstructed values in Fig. 8. In spite of the scattering nature of the material and the incoherent light sources, the results demonstrate the ability to obtain phase information and quantitatively locate the axial position of a fluorescent light source within the medium.

5 Conclusion and Outlook

A method for reconstructing the 3-D position of a fluorescent light source is reported. The reconstruction of the axial position relies on the knowledge of the phase of the fluorescent wave fronts. It is demonstrated that a shearing setup based on a Michelson interferometer is able to record this information in spite of the limited temporal and absent spatial coherence of fluorescent light. As opposed to methods such as confocal fluorescence microscopy or multiphoton microscopy, a model-based reconstruction involving computational processing of the recorded images is needed. It has to be mentioned that the main purpose of the method is the reconstruction of the axial position of a fluorescent light source rather than a complete imaging of a sample volume. A reconstruction procedure based on a phase-shifting procedure is developed, and a simple analytical relation between the properties of the sheared wave front and the vertical position of the fluorescent light source is derived. Application of the phase shifting procedure allows a separation of the interference signal from the incoherent background. In an earlier publication, the qualitative agreement between the recorded interference patterns and fringe contrasts and the respective results obtained by Monte Carlo simulations has been shown.²⁴ In a next step, these simulation results could also be used to refine the model-based reconstruction by taking into account the spatial extent of the fluorescent light sources and possible *a priori* knowledge about the distributions of the scatterers in the material. An inverse problem would

arise, in which the experimentally obtained intensity distributions would then have to be matched to the numerical results.

For the purpose of experimentally validating the proposed method, phantoms with precisely characterized optical properties have been examined. The measurements at these phantoms demonstrate the depth-resolved detection of fluorescent light for materials with moderate scattering coefficients of 2/mm in depths of the order of hundred micrometers with a resolution in the micron range and a relative accuracy in the range of 10%. A large part of the remaining uncertainty is ascribed to the nature of the lab setup, which in its current state has mainly been optimized for flexibility, large measurement range, and ease of handling by operating in the visible range and at moderate numerical aperture.

Depending on the application, there is a potential and need for optimization: increased axial and lateral resolution can be achieved by working at higher numerical apertures. This affects both illumination and detection: the intersecting angles between the two interfering beams as well as the sensitivity of the detection increase due to a larger magnification. This could be relevant if the method is to be used to add depth information to a fluorescence imaging setup aiming at the investigation of small biological structures like cells. To extend the penetration depth in scattering materials, there are several options for improvement. One could replace rhodamine 6G by a fluorophore absorbing and emitting in the infrared region. The reduced strength of the fluorescence could be compensated by the decrease in the scattering coefficient for longer wavelengths. In addition, one could tune the concentrations of fluorophores in certain limits or increase use of a light source with a larger power in the spectral region close to the absorption maximum of the fluorophore.

With such enhancements concerning the maximal penetration, depth, and adaption of the fluorophore, the method could have the potential to complement existing fluorescence-based methods in *in vivo* diagnostics. In comparison with the scanning procedures of multiphoton fluorescence microscopy^{4,7} or fluorescence lifetime imaging,⁶ one could profit from a large measurement range as measurements are also possible for light sources several hundred micrometers away from the focus. The results presented in this work as well as previous simulation results²⁴ indicate that the limiting factor for the maximal depth is the detected number of photons and not the signal-to-noise-ratio, since even for the largest depths a sufficient contrast is achieved.

In addition to the field of *in vivo* diagnostics, the method could be applied to measurement tasks where the investigation of structures beyond the surface of materials is required. Fluorescent marker materials are used for the detection of microcracks in human bone,²⁶ where depth information could substantially facilitate the identification and classification, and in monitoring the erosion of biodegradable materials.²⁷ In the investigations of the penetration of certain substances into the skin, e.g., cosmetic products,²⁸ the method could enable a non-invasive access to the penetration depth. If the conditions allow the introduction of fluorophores, shearing interferometry could also serve as an alternative to OCT for the detection of defects or the measurements of deformations.²⁹

Disclosures

The authors declare no competing interests.

Acknowledgments

This work has been funded by the Landesstiftung Baden-Wuerttemberg within the project “Tiefenaufgelöste Fluoreszenzdetektion in streuenden Medien” (FluoTis). We thank our partners at ILM for the production of the phantoms and the collaboration during the project.

References

1. C. Balch et al., “Final version of the American Joint Committee on Cancer staging system for cutaneous melanoma,” *J. Clin. Oncol.* **19**(16), 3635–3648 (2001).
2. S. Keereweer et al., “Optical image-guided surgery—where do we stand?” *Mol. Imaging Biol.* **13**(2), 199–207 (2011).
3. W. Drexler and J. G. Fujimoto, Eds., *Optical Coherence Tomography, Biological and Medical Physics, Biomedical Engineering*, 1st ed., Springer-Verlag, Berlin Heidelberg (2008).
4. F. Helmchen and W. Denk, “Deep tissue two-photon microscopy,” *Nat. Methods* **2**, 932–940 (2005).
5. P. A. Santi, “Light sheet fluorescence microscopy: a review,” *J. Histochem. Cytochem.* **59**(2), 129–138 (2011).
6. J. W. Borst and A. J. W. G. Visser, “Fluorescence lifetime imaging microscopy in life sciences,” *Meas. Sci. Technol.* **21**(10), 102002 (2010).
7. S. Paddock, “Principles and practices of laser scanning confocal microscopy,” *Mol. Biotechnol.* **16**(2), 127–149 (2000).
8. J. Mertz and J. Kim, “Scanning light-sheet microscopy in the whole mouse brain with HiLo background rejection,” *J. Biomed. Opt.* **15**(1), 016027 (2010).
9. M. A. A. Neil, R. Juškaitis, and T. Wilson, “Method of obtaining optical sectioning by using structured light in a conventional microscope,” *Opt. Lett.* **21**, 1905–1907 (1997).
10. J. Rosen and G. Brooker, “Digital spatially incoherent fresnel holography,” *Opt. Lett.* **32**, 912–914 (2007).
11. J. Rosen and G. Brooker, “Non-scanning motionless fluorescence three-dimensional holographic microscopy,” *Nat. Photonics* **2**, 190–195 (2008).
12. Y. Wan, T. Man, and D. Wang, “Incoherent off-axis Fourier triangular color holography,” *Opt. Express* **21**, 8565–8573 (2014).
13. M. K. Kim, “Full color natural light holographic camera,” *Opt. Express* **21**, 9636–9642 (2013).
14. J.-C. Chanteloup, “Multiple-wave lateral shearing interferometry for wave-front sensing,” *Appl. Opt.* **44**, 1559–1571 (2005).
15. P. Bon et al., “Quadriwave lateral shearing interferometry for quantitative phase microscopy of living cells,” *Opt. Express* **17**, 13080–13094 (2009).
16. P. Bon et al., “Three-dimensional nanometre localization of nanoparticles to enhance super-resolution microscopy,” *Nat. Commun.* **6**, 7764 (2015).
17. J. Chu and S.-W. Kim, “Absolute distance measurement by lateral shearing interferometry of point-diffracted spherical waves,” *Opt. Express* **14**, 5961–5967 (2006).
18. D. S. Mehta et al., “Distance measurement with extended range using lateral shearing interferometry and Fourier transform fringe analysis,” *Opt. Eng.* **44**(6), 063602 (2005).
19. R. Kubin and A. Fletcher, “Fluorescence quantum yields of some rhodamine dyes,” *J. Lumin.* **27**(4), 455–462 (1983).
20. J. Schwider et al., “Digital wave-front measuring interferometry: some systematic error sources,” *Appl. Opt.* **21**, 3421–3432 (1983).
21. P. Hariharan, B. F. Oreb, and T. Eiju, “Digital phase-shifting interferometry: a simple error-compensating phase calculation algorithm,” *Appl. Opt.* **26**, 2504–2506 (1987).
22. R. M. Goldstein, H. A. Zebker, and C. L. Werner, “Satellite radar interferometry: two-dimensional phase unwrapping,” *Radio Sci.* **23**(4), 713–720 (1988).
23. M. P. Rimmer and J. C. Wyant, “Evaluation of large aberrations using a lateral-shear interferometer having variable shear,” *Appl. Opt.* **14**, 142–150 (1975).
24. J. Schindler et al., “Resolving the depth of fluorescent light by structured illumination and shearing interferometry,” *Proc. SPIE* **9718**, 97182H (2016).
25. P. Krauter et al., “Optical phantoms with adjustable subdiffusive scattering parameters,” *J. Biomed. Opt.* **20**(10), 105008 (2015).
26. T. C. Lee, E. R. Myers, and W. C. Hayes, “Fluorescence-aided detection of microdamage in compact bone,” *J. Anat.* **193**(2), 179–184 (1998).
27. N. Artzi et al., “In vivo and in vitro tracking of erosion in biodegradable materials using non-invasive fluorescence imaging,” *Nat. Mater.* **10**, 896–896 (2011).
28. A. Teichmann et al., “An in vivo model to evaluate the efficacy of barrier creams on the level of skin penetration of chemicals,” *Contact Dermatitis* **54**(1), 5–13 (2006).
29. Y. Zhang et al., “Measurement of depth-resolved thermal deformation distribution using phase-contrast spectral optical coherence tomography,” *Opt. Express* **23**, 28067–28075 (2015).

Johannes Schindler received his diploma degree in physics from Karlsruhe Institute of Technology in 2012. Since July 2012, he has been a PhD student in the Institut für Technische Optik at the University of Stuttgart. His main research interests comprise interferometry, model-based measurements methods, and asphere and freeform metrology.

Biographies for the other authors are not available.